*Pure Appl. Chem.*, Vol. 81, No. 7, pp. 1279–1296, 2009.
doi:10.1351/PAC-CON-08-09-07


# Vanadium-salen and -salan complexes: Characterization and application in oxygen-transfer reactions*

Pedro Adão[1], Mannar R. Maurya[2], Umesh Kumar[2], Fernando Avecilla[3], Rui T. Henriques[1], Maxim L. Kusnetsov[1], João Costa Pessoa[1,‡], and Isabel Correia[1,‡]

*[1]Centro Química Estrutural, Instituto Superior Técnico, TU Lisbon, Av. Rovísco Pais, 1049-001 Lisbon, Portugal; [2]Department of Chemistry, Indian Institute of Technology, Roorkee 247667, India; [3]Departamento de Química Fundamental, Universidade da Coruña, Campus da A Zapateira, 15071, A Coruña, Spain*

*Abstract*: Salen complexes are a versatile and standard system in oxidation catalysis. Their reduced derivatives, called salan, share their versatility but are still widely unexplored. We report the synthesis of a group of new vanadium-salen and -salan complexes, their characterization and application in the oxidation of simple organic molecules with $H_2O_2$. The ligands are derived from pyridoxal and chiral diamines (1,2-diaminocyclohexane and 1,2-diphenylethylenediamine) and were easily obtained in high yields. The $V^{IV}$ complexes were prepared and characterized in the solid state (Fourier transform infrared, FTIR, and magnetic properties) and in solution by spectroscopic techniques: UV–vis, circular dichroism (CD), electron paramagnetic resonance (EPR), and $^{51}V$ NMR, which provide information on the coordination geometry. Single crystals suitable for X-ray diffraction studies were obtained from solutions containing the $V^{IV}$-pyr(*S*,*S*-chan) complex: $[V^{V}O\{pyr(S,S\text{-}chen)\}]_2(\mu\text{-}O)_2{\cdot}2(CH_3)_2NCHO$, where the ligand is the "half" Schiff base formed by pyridoxal and 1*S*,2*S*-diaminocyclohexane. The dinuclear species shows a $OV^{V}(\mu\text{-}O)_2V^{V}O$ unit with tridentate ligands and two μ-oxo bridges. The $V^{IV}$ complexes of the salan-type ligands oxidize in organic solvents to a $V^{V}$ species, and the process was studied by spectroscopic techniques. The complexes were tested as catalysts in the oxidation of styrene, cyclohexene, and cumene with $H_2O_2$ as oxidant. Overall, the V-salan complexes show higher activity than the parent V-salen complexes and are an alternative ligand system for oxidation catalysis.

*Keywords*: salen; salan; vanadium complexes; oxygen-transfer reactions.

## INTRODUCTION

Traditional methods for the oxidation of organic substrates involve the use of stoichiometric amounts of high-valent metal compounds, such as $CrO_3$. Unfortunately, these reactions generate large amounts of solid waste and are becoming less popular in the face of growing environmental concerns. Besides being environmentally more benign, catalytic oxidation of organic compounds with oxidants such as

*Paper based on a presentation at the 6th International Symposium on Chemistry and Biological Chemistry of Vanadium, 17–19 July 2008, Lisbon, Portugal. Other presentations are published in this issue, pp. 1187–1330.

‡Corresponding authors

molecular oxygen and hydrogen peroxide is less economically wasteful than the traditional methods and is now an important procedure in both the laboratory scale and industry.

Salen complexes are a standard system in coordination chemistry and found use as efficient catalysts for oxo transfer reactions [1,2] and other processes [3,4]. They are tetradentate dianionic ligands similar to porphyrins, and among their advantages is the ease of preparation, which allows the tuning of their electronic and steric properties through modular synthesis. This is especially advantageous in catalysis where solubility, activity, and selectivity are important issues, and therefore their metal complexes have been widely applied as catalysts in oxidation reactions with moderate-to-good yields. The first use of metal salen complexes for catalytic asymmetric reactions was probably the vanadyl-catalyzed oxidation of sulfides reported by Fujita [5]. Later came the breakthrough with the work of Jacobsen [6] and Katsuki [7], which developed the enantioselective epoxidation of unfunctionalized alkenes using chiral Mn(salen) complexes as catalysts. Since then, an extremely wide variety of reactions catalyzed by salen complexes have been investigated [1–4]. However, many types of reactions remain where selectivity and catalyst stability, activity, and recyclability need to be improved before the catalytic systems become suitable for the synthesis of fine chemicals. Moreover, in solution salen ligands have the disadvantage of the hydrolysis of the C=N bond, particularly in water-containing solvents [8,9].

The reduced counterparts of the salen compounds, known as salan-type ligands or tetrahydrosalen, are much less studied. The presence of two $sp^3$-hybridized nitrogens instead of $sp^2$ confers them higher flexibility and may also increase their stability toward hydrolysis. They tend to coordinate to metal ions in high oxidation states forming *cis*-α or *cis*-β $C_2$ symmetry octahedral complexes, while due to the planar nature of the salen ligands their octahedral complexes usually adopt *trans* geometry. These characteristics have led to the recent development of salan chemistry and in particular to the application of their metal complexes as catalysts: Kol et al. applied with success zirconium-salan complexes in polymerizations [10]; Katsuki is responsible for most of the work done with Ti(salan) complexes in sulfoxidations and epoxidations [11], and his group also reported the potential of an $Fe^{II}$-salan-$H_2O_2$ (aq) system in the sulfoxidation of thioanisole, with ee's as high as 96 % [12]. Other successful recent examples are the asymmetric pinacol coupling of aryl aldehydes with a $Mo^{IV}$-salan system [13]; the asymmetric Henry reaction catalyzed by a $Cu^{I}$-salan complex [14]; the addition of diethylzinc to benzaldehyde catalyzed by a Ti(salan) complex [15]; and the asymmetric oxidation of sulfides catalyzed by V-salan complexes with $H_2O_2$ with good yields and high enantioselectivities are further examples [16].

In this work, we report the synthesis, characterization, and catalytic potential of chiral V-salen and -salan complexes derived from pyridoxal and chiral diamines: 1,2-diaminocyclohexane and 1,2-diphenylethylenediamine. Our group has been studying salan complexes for several years [8,9,17,18]. We reported studies on the solution speciation of salan-type ligands with $V^{IV}$ and $V^{V}$, $Cu^{II}$, $Ni^{II}$, and $Zn^{II}$. Our aim was to study their coordination ability and to identify species and binding modes formed in solution. Several single-crystal X-ray structures were obtained of both the ligands and the metal complexes, and in all cases the flexibility of the ligand was evidenced. The speciation studies (by pH-potentiometry and spectroscopic techniques) showed the higher stability of the salan complexes (when compared to the salen) due to the presence of amines instead of imines. These results led us to develop other V-salan complexes, to study their structural properties, and to test them in oxidation catalysis; this is our second report [19] on the catalytic activity of V-salan complexes. Although the complexes are chiral and could induce asymmetry in catalytic reactions, this report presents only its application as catalysts in simple organic reactions with $H_2O_2$, with no particular objective concerning the stereoselectivity of products.

## EXPERIMENTAL SECTION

### Materials

All chemicals used for the synthetic work were obtained from Merck, Sigma-Aldrich, or Rocc and were of reagent grade and used without further purification.

### Resolution of racemic cyclohexanediamine

The amine enantiomers were separated according to a literature procedure [20]. The tartarate salt was used directly in the preparation of the ligands.

### Synthesis of the ligands

**pyr(*R*,*R*-chen) 1:** The compound was prepared similarly to a literature procedure [21] used for salen compounds by the reaction of pyridoxal hydrochloride with the optically active diamine (2:1) in methanol. Yield: 98 %. Anal. calcd. for $C_{22}H_{28}N_4O_4 \cdot 0.5H_2O$: C, 62.69; H, 6.93; N, 13.29. Found: C, 62.2; H, 7.2; N, 13.5. 1H NMR-DMSO-$d_6$: 1.76, 1.94, 2.01, 2.19 [8H, m, –C$H_2$–], 2.77 [6H, s, Ar–C$H_3$], 3.87 [2H, s, $CH_2$C*H*–N], 4.83 [4H, m, –C$H_2$–OH], 8.19 [2H, s, aromatic], 9.13 [2H, s, C*H*=N]. FTIR: ν(C=N) = 1628 cm−1. UV–vis in $H_2O$: $\lambda_{max}$/nm ($\varepsilon$/$M^{-1}$ $cm^{-1}$) 244 (1250), 312 (1090), and 392 (265).

**pyr(*R*,*R*-dpen) 2:** The procedure was similar to **1**. Yield: 97 %. Anal. calcd. for $C_{30}H_{30}N_4O_4 \cdot 0.5H_2O$: C, 69.41; H, 5.92; N, 10.79; found: C, 69.1; H, 6.3; N, 10.6; $^1$H NMR-DMSO-$d_6$: 2.45 [6H, s, Ar–C$H_3$], 4.62 [4H, m, –C$H_2$–OH], 5.35 [2H, s, PhC*H*–N], 7.36 [10H, m, aromatic], 7.93 [2H, s, aromatic], 9.01 [2H, s, C*H*=N]. FTIR: ν(C=N) = 1626 $cm^{-1}$. UV–vis in DMSO: $\lambda_{max}$/nm ($\varepsilon$/$M^{-1}$ $cm^{-1}$) 258 (1950), 340 (698), and 418 (687).

**pyr(*R*,*R*-chan) 3:** pyr(*R*,*R*-chen) was dissolved in MeOH and a slight excess of $NaBH_4$ was slowly added. The reduction was considered complete when the solution became colorless. The pH was adjusted to 1–1.5 with HCl 4 M and then the pH was re-adjusted to 8 with NaOH 4 M, and a white solid precipitated which was washed with EtOH and dried. Recrystallization with EtOH yielded a pale yellow solid. Yield: 89 %. Anal. calcd. for $C_{22}H_{34}N_4O_4Cl_2 \cdot 7.5H_2O$: C, 42.31; H, 7.91; N, 8.97; found: C, 42.5; H, 7.5; N, 8.6; $^1$H NMR-$D_2O$ (pH ~4.3): 1.43, 1.87, 2.48, [8H, m, –C$H_2$–], 2.76 [6H, s, Ar–C$H_3$], 4.43, 4.46, 4.58, 4.62 [6H, dd, C$H_2$–$N^+H_2$,$CH_2$C*H*–$N^+H_2$ ], 4.96 [4H, m, –C$H_2$–OH], 8.27 [2H, s, aromatic]. UV–vis in $H_2O$: $\lambda_{max}$/nm ($\varepsilon$/$M^{-1}$ $cm^{-1}$) 218 (2280), 250 (589), 296 (710), and 324 (915).

**pyr(*S*,*S*-dpan) 4:** The compound was obtained by the same procedure used for **3**, being also converted to its HCl salt. A light yellow solid was obtained. Yield: 90 %. Anal. calcd. for $C_{30}H_{38}N_4O_4Cl_4 \cdot 2.5H_2O$: C, 51.07; H, 6.14; N, 7.94; found: C, 51.4; H, 5.9; N, 7.7; $^1$H NMR-$D_2O$ (pH ~4.3): 2.51 [6H, s, Ar–C$H_3$], 4.26 [4H, s, ArC$H_2$–$N^+$H2], 4.44 [4H, s, PhC*H*–$N^+$H2], 4.60 [4H, s, –C$H_2$–OH], 7.20 [10H, m, aromatic], 8.01 [2H, s, aromatic]. UV–vis in $H_2O$: $\lambda_{max}$/nm ($\varepsilon$/$M^{-1}$ $cm^{-1}$) 210 (2680), 246 (sh, 509), 292 (1030), and 324 (583).

### Synthesis of the oxovanadium(IV) complexes

A general procedure was applied for the synthesis of the oxovanadium(IV) complexes, and all reactions were carried out under nitrogen atmosphere. The ligand (1 equiv) was dissolved in MeOH, then 1.1 equiv of $VOCl_2$ (50 % aqueous solution) were added and the pH was adjusted to 7 using NaOH 1 M. The desired oxovanadium(IV) complex precipitated, was filtered, washed with MeOH and water, and dried under vacuum.

**{$V^{IV}$O[pyr(*R*,*R*-chen)]} 5:** An orange–brown solid was obtained. Yield: 61 %. Anal. calcd. for $C_{22}H_{26}N_4O_5V \cdot 3H_2O$: C, 49.72, H, 6.07; N, 10.54; found: C, 49.7; H, 6.1; N, 10.7. FTIR:

ν(C=N) = 1626 $cm^{-1}$, ν(V=O) = 888 $cm^{-1}$. UV–vis in DMSO: $\lambda_{max}$/nm ($\varepsilon$/$M^{-1}$ $cm^{-1}$): 270 (sh, 14 850), 380 (7700), 574 (131), and 738 (sh, 55).

**{$V^{IV}O$[pyr(*R*,*R*-dpen)]} 6:** A light green solid was obtained. Yield: 76 %. Anal. calcd. for $C_{30}H_{28}N_4O_5V{\cdot}2H_2O$: C, 58.92, H, 5.27; N, 9.16; found: C, 58.9; H, 5.1; N, 9.1. FTIR: ν(C=N) = 1625 $cm^{-1}$, ν(V=O) = 990 $cm^{-1}$. UV–vis in DMSO: $\lambda_{max}$/nm ($\varepsilon$/$M^{-1}$ $cm^{-1}$) 280 (sh, 11 040), 386 (6180), 586 (95), and 746 (sh, 48).

**{$V^{IV}O$[pyr(*R*,*R*-chan)]} 7:** A pink solid was obtained. Yield: 54 %. Anal. calcd. for $C_{22}H_{30}N_4O_5V{\cdot}2.5H_2O$: C, 50.19, H, 6.79; N, 10.64; found: C, 50.4; H, 6.6; N, 10.6. FTIR: ν(V=O) = 885 $cm^{-1}$. $^{51}V$ NMR-DMSO (4 h after dissolution in the presence of air): –525 ppm (br).

**{$V^{IV}O$[pyr(*S*,*S*-dpan)]} 8:** A brown solid was obtained with minor inorganic impurities, though the carbon/nitrogen ratio is 12.01, as expected. Yield: 80 %. Anal. calcd. for $C_{30}H_{32}N_4O_5V{\cdot}2.5H_2O$: C, 57.69, H, 5.97; N, 8.97. Found: C, 58.0; H, 6.0; N, 8.9. FTIR: ν(V=O) = 930 or 891 $cm^{-1}$. $^{51}V$ NMR-DMSO (4 h after dissolution in the presence of air): –528 ppm (br).

## Synthesis of the $V^V$ complexes

The procedure was the same for all complexes: 0.5 g of the parent $V^{IV}O$ complex was dissolved in 20 ml of $CH_2Cl_2$ under vigorous stirring and air. After 24 h, the solution was dark red–brown. The solvent was then evaporated to dryness, and the residue was washed with water, small amounts of MeOH and *n*-hexane, and dried under vacuum.

**{$V^{V}O$[pyr(*R*,*R*-chan)]}$_2$(μ-O) 9:** Due to the low solubility of **7** in $CH_2Cl_2$, a 1:1 mixture of MeOH/$CH_2Cl_2$ was used. A dark red solid was obtained. Yield: 65 %. Anal. calcd. for $C_{44}H_{62}N_8O_{11}V_2Cl{\cdot}6H_2O$: C, 48.53, H, 6.85; N, 10.29; found: C, 48.8; H, 6.5; N, 10.0. FTIR: ν(V=O) = 931 $cm^{-1}$. $^{51}V$ NMR-DMSO: –519 ppm (br).

**{$V^{V}O$[pyr(*R*,*R*-dpan)]}$_2$(μ-O) 10:** A dark brown solid was obtained. Yield: 30 %. Anal. calcd. for $C_{60}H_{66}N_8O_{11}V_2{\cdot}6H_2O$: C, 56.07, H, 6.12; N, 8.72; found: C, 55.9; H, 5.9; N, 8.3. FTIR: ν(V=O) = 923 $cm^{-1}$. $^{51}V$ NMR-DMSO: –525 ppm (br).

**{[$V^{V}O$[pyr(*S*,*S*-chen)]}$_2$(μ-O)$_2$·2$(CH_3)_2$NCOH 11:** Complex **7** was dissolved in DMF, and the resulting purple solution was left under air to evaporate slowly. The solution turned red as a result of $V^{IV}O$ oxidation. After ca. 6 weeks, the solution became orange and yellow needles were formed. $^{51}V$ NMR-MeOH: –500 ppm.

## Physical and spectroscopic studies

IR spectra were recorded with a BioRad FTS 3000 MX FTIR spectrometer. Visible spectra were recorded either with a Hitachi U-2000 or a Simadzu UV-2401PC spectrophotometer. The temperature was controlled at 25 °C using thermostatized sample compartments with a Julabo F12 thermostatic bath circulators. The electron paramagnetic resonance (EPR) spectra were recorded at 77 K (on glasses made by freezing solutions in liquid nitrogen) with a Bruker ESP 300E X-band spectrometer. The $^1H$ NMR spectra were obtained on a Bruker Avance+ 400 Mhz Spectrometer, and the $^{51}V$ NMR on a Varian Unity Inova 300 instrument operating at 131.404 MHz, using a 5-mm broad-band probe and a controlled temperature unit set at 25 ± 1 °C. The identity of the catalytic products was confirmed using a GC/MS model Perkin-Elmer, Clarus 500 and comparing the fragments of each product with the library available. A Thermax Nicolet gas chromatograph with a HP–1 capillary column (30 m × 0.25 mm × 0.25 μm) was used to analyze the reaction products. Each catalytic experiment was repeated twice for the validation of the data.

### EPR spectroscopy

The $V^{IV}O$ EPR spectra were simulated using a program from Rockenbauer [22]. The EPR spectra help to elucidate which groups coordinate in solution [23]. For the $V^{IV}O$ systems, we used the additivity rule to estimate the hyperfine coupling constant $A_{||}^{est}$, based on the contributions $A_{||,i}$ of each of the four equatorial donor groups [$A_{||}^{est} = \Sigma A_{||,i}$ ($i$ = 1 to 4)]. The estimated accuracy of $A_{||}^{est}$ is $\pm 3 \times 10^{-4}$ $cm^{-1}$ [23]. This data can be used to establish the most probable binding mode of the complexes formed, but care must be taken as the contributions of the donor groups to the hyperfine coupling may depend on their orientation [24], or charge of the ligand [25]. The influence of the axial donor groups (if any) was not taken into account, since it is considered not relevant in the present systems [26].

### $^{1}H$ and $^{51}V$ NMR spectroscopy

All samples for NMR studies were prepared at room temperature. The solutions containing the $V^{V}$ complexes were prepared by weighting the adequate amount of the complex and dissolving it in the solvent to obtain $^{51}V$ NMR spectra. The $^{1}H$ and $^{51}V$ NMR chemical shifts were referenced relative to TSS [sodium 3-(trimethylsilyl)propane sulfonate] at 0 ppm, and to neat $VOCl_3$ at 0 ppm, respectively. $^{51}V$ NMR acquisition parameters were: 33 kHz spectral width, 30 μs pulse width, 1 s acquisition time, and 50 Hz line broadening.

### X-ray crystal structure determination

Three-dimensional X-ray data for **11** were collected on a Bruker Kappa X8Apex CCD diffractometer by the $\phi$-$\omega$ scan method. The data was collected at low temperature. Reflections were measured from a hemisphere of data collected of frames each covering 0.3° in $\omega$. Of the 17853 reflections measured, all of which were corrected for Lorentz and polarization effects, and for absorption by semi-empirical methods based on symmetry-equivalent and repeated reflections, 6053 independent reflections exceeded the significance level $|F|/\sigma(|F|) > 4.0$. Complex-scattering factors were taken from the program package SHELXTL [27]. The structure was solved by direct methods and refined by full-matrix least-squares methods on $F^2$. The non-hydrogen atoms were refined with anisotropic thermal parameters in all cases. The hydrogen atoms were included in calculated positions and refined by using a riding mode for all atoms. A final difference Fourier map showed no residual density outside: 0.616, –0.798 e.$Å^{-3}$. CCDC 700857 contains the supplementary crystallographic data for **11**. This data can be obtained free of charge from the Cambridge Crystallographic Data Centre via <www.ccdc.cam.ac.uk/data_request/cif>. Crystal data and details on data collection and refinement are summarized in the Supplementary Information.

### Catalytic activity studies

All catalytic reactions for the oxidation of styrene, cyclohexene, and cumene were carried out using 50-ml double-neck reaction flasks fitted with a septum and a water condenser. In a typical reaction (see discussion), styrene (0.52 g, 5 mmol), aqueous 30 % $H_2O_2$ (1.13 g, 10 mmol), and the catalyst (0.10 mmol) were mixed in $CH_3CN$ (10 ml) and the reaction was carried out at 80 °C, with stirring. During the course of the reaction, 0.5 ml of the reaction mixture was withdrawn every half-hour, extracted with petroleum ether (5 × 2 ml), and analyzed quantitatively by gas chromatography.

## RESULTS AND DISCUSSION

### Ligand synthesis and characterization

The synthesis of the salen-type compounds involved the reaction of pyridoxal with the chiral diamines, (1*R*,2*R*- and 1*S*,2*S*-diaminocyclohexane or 1*S*,2*S*-diphenylethylenediamine). Their formula and abbreviations used are shown below. The synthesis of the salan-type ligands involved the reduction of the salen parent compounds with $NaBH_4$ and their conversion to the HCl salts. They were prepared in high yields (>90 %), gave satisfactory elemental analysis, and were characterized by spectroscopic techniques: $^1$H NMR, FTIR, UV, and circular dichroism (CD).

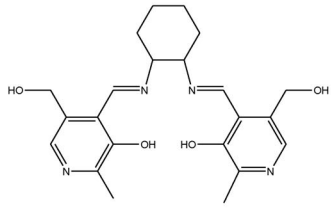

**1 pyr(chen)**

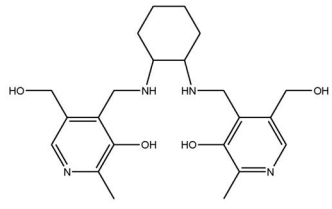

**3 pyr(chan)**

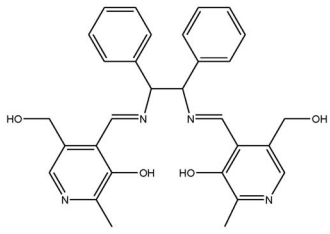

**2 pyr(dpen)**

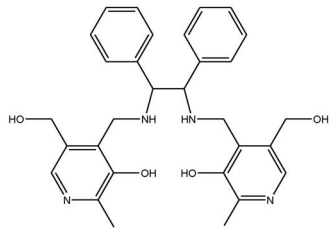

**4 pyr(dpan)**

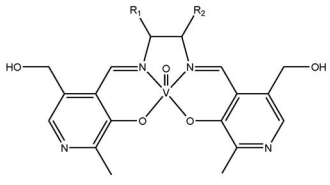

**5** $R_1,R_2 = -(CH_2)_4-$
**6** $R_1,R_2 = Ph$

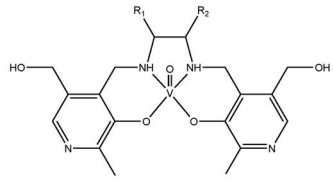

**7** $R_1,R_2 = -(CH_2)_4-$
**8** $R_1,R_2 = Ph$

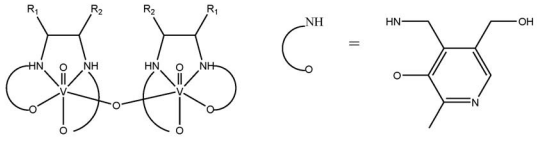

**9** $R_1,R_2 = -(CH_2)_4-$
**10** $R_1,R_2 = Ph$

In the $^1$H NMR spectra, the peaks attributed to the $CH_2$–N groups of pyran-type compounds appear at $\delta \sim 4$ ppm and the CH=N peaks are not detected, confirming the reduction of the imine bonds. The FTIR spectra also do not show the ν(C=N) band, and the ν(N–H) appears under a broad band centered at ca. 3400 cm$^{-1}$, due to the presence of water molecules and the phenolic OH groups. In the electronic absorption spectra (see Experimental section), the C=N bands, which in the spectra of the parent pyren ligands are responsible for the $n \rightarrow \pi^*$ and the $\pi \rightarrow \pi^*$ transitions (at ca. 300–400 nm) do not exist. The UV transitions observed are due to the $\pi \rightarrow \pi^*$ transitions associated with the aromatic rings.

### Synthesis and characterization of the V complexes

The reaction of compounds **1–4** with $VOCl_2$ leads to the formation of $V^{IV}O$ complexes with a $N_2O_2$ binding mode, in moderate yields. The complexes were characterized by elemental analysis and spectroscopic techniques. Compounds **9** and **10** were obtained by aerobic oxidation of the parent $V^{IV}O$ complexes. The elemental analysis and the spectroscopic characterization of the $V^V$-pyran complexes fit well with a dinuclear formulation with two $V^V$ centers and one μ-oxo bridge. The IR spectra show that most of the $V^{IV}O$ complexes present the ν(V=O) at ca. 880 cm$^{-1}$ (see Experimental section, for **8**, the assignment is not straightforward). These low ν(V=O) values indicate V=O···V=O interactions. The binding of an $O_{oxo}$ to an adjacent vanadium, *trans* to its vanadyl O-atom, lengthens and weakens the bond, thereby lowering the V=O stretching frequency. This is also in agreement with the EPR spectra, which immediately after dissolution of the complexes in dimethylsulfoxide (DMSO) show some aggregation of the molecules (see below). Complex **6** is monomeric in the solid state with the ν(V=O) at ca. 990 cm$^{-1}$. The Schiff-base complexes show ν(C=N) bands at 1625 cm$^{-1}$, and the ν(C–O) bands show up in the range 1240–1290 cm$^{-1}$.

### Electronic absorption spectra

The $V^{IV}$-pyren complexes **5** and **6** show two bands in the visible region which can be assigned to band I ($d_{xy} \rightarrow d_{xz}$, $d_{yz}$) and II ($d_{xy} \rightarrow d_{x2-y2}$), and band III is below an intense charge-transfer (CT) band at ca. 380 nm (see Experimental section). The $V^{IV}$ complexes of the pyran derivatives are not stable when dissolved in organic solvents (DMSO or $CH_2Cl_2$). The solutions turn strong red–brown with time, and addition of a reducing agent (sodium dithionite or ascorbic acid) reverts the solution to its original color. When complex **7** is dissolved in DMSO, the spectrum shows only a band at 482 nm (shoulder, $\varepsilon$ = 275 M$^{-1}$ cm$^{-1}$), under a strong band tailoring from the UV. Upon addition of excess $Na_2S_2O_4$, new bands appear at 770 ($\varepsilon$ = 125 M$^{-1}$ cm$^{-1}$) and 506 nm (shoulder, $\varepsilon$ = 250 M$^{-1}$ cm$^{-1}$). For **8**, the behavior is very similar and the spectroscopic data obtained after addition of the reducing agent is collected in the Supplementary Information. The same behavior was observed with complexes from salicyladehyde derivatives instead of pyridoxal [19], and all data supports the relatively easy oxidation of the $V^{IV}O$ complex into a $V^V$ species by molecular oxygen. The transition at 482 nm is considered a CT from a pπ orbital on the phenolate oxygen lone-pair to the empty 3d-orbitals of the V atom [28,29]. This is also corroborated by the spectra of the $V^V$ complexes **9** and **10**, which show features that are similar to those observed upon oxidation of the $V^{IV}$ solutions, namely, the strong CT band centered at 500 nm. Other spectroscopic studies confirmed this assumption and will be detailed below.

### EPR

The X-band 1$^{st}$ derivative EPR spectra of frozen solutions (77 K) of the vanadium complexes dissolved in DMSO were measured and simulated (whenever possible) [22], and the spin-Hamiltonian parameters are collected in Table 1. The spectra are either axial or show a small rhombic distortion (complex **7**).

For complexes of this type in an octahedral environment (considering the coordination of a solvent molecule), three binding modes can be envisioned, which are depicted in Scheme 1.

**Table 1** Spin-Hamiltonian parameters calculated for the EPR spectra measured in DMSO.

| Compound | $g_x$, $g_y$ (or $g_\perp$) | $A_x$, $A_y$ (or $A_\perp$) $\times 10^4$ cm$^{-1}$ | $g_z$ (or $g_{//}$) | $A_z$ (or $A_{//}$) $\times 10^4$ cm$^{-1}$ | Binding mode ($A_{//}^{est} \times 10^4$ cm$^{-1}$) |
|---|---|---|---|---|---|
| **5** | 1.978 | 52.8 | 1.957 | 158.8 | *cis*-α (163.5) |
| **6** | – | – | 1.957 | 159.6 | *cis*-α (163.5) |
| **7** | 1.979, 1.973 | 51.2, 51.3 | 1.957 | 158.3 | *trans* (157.9) or *cis*-α (159.7) |
| **8** | 1.973 | 54.9 | 1.943 | 163.5 | *cis*-β (160.9) |
| | 1.976 | 53.4 | 1.954 | 159.7 | *trans* (157.9) or *cis*-α (159.7) |

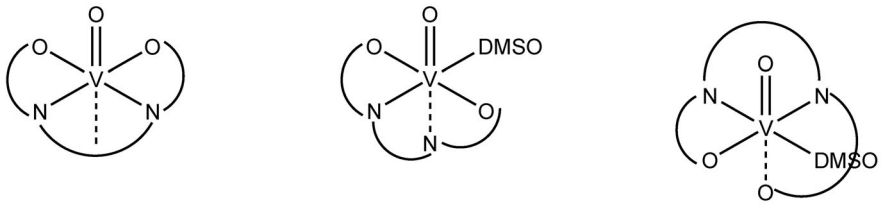


**trans** **cis-α** **cis-β**

**Scheme 1** Possible binding modes for $V^{IV}O$ complexes considering an octahedral geometry and coordination of a solvent molecule.

For complexes **5** and **6**, the parameters fit well with a *cis*-α-type binding mode involving coordination of one of the imine bonds in the apical position, and a DMSO molecule in the equatorial position for which a value of $A_{//}^{est} = 163.5 \times 10^{-4}$ cm$^{-1}$ is obtained. Immediately after dissolution of complexes **7** and **8** the spectra show the presence of a broad band, which is due to aggregation of the molecules in the solid state. The solutions change with time, this broad band progressively disappearing, but the features and spin-Hamiltonian parameters for the $V^{IV}O$ species remain the same. For complexes **7** and **8**, the parameters fit well with binding modes of the type *trans* or *cis*-α for which $A_{||}^{est}$ values of $157.9 \times 10^{-4}$ and $159.7 \times 10^{-4}$ cm$^{-1}$ are obtained, respectively. Therefore, it is not possible to assign the spectra to a particular structure in solution. However, when dissolved in DMSO, complex **8** shows the presence of two distinct $V^{IV}$ complexes. These should correspond to different isomers, which coexist in solution, one of them with a binding mode of the *cis*-β-type ($A_{||}^{est} = 160.9 \times 10^{-4}$ cm$^{-1}$).

The oxidation process was also studied by EPR. Complex **7** was dissolved in DMSO (ca. 10 mM, $t = 0$), and the solutions were left under air. EPR samples were taken and frozen at different time intervals: 0, 1, and 4 h, and the spectra were measured at 77 K, keeping the acquisition parameters constant. The intensity of the central lines of the EPR spectra can give an estimate of the amount of $V^{IV}$ present in solution, and this progressively decreases with time, confirming that the complexes are being oxidized (Fig. 1a). We can also observe that the $V^{IV}O$ species present in solution, as the oxidation process proceeds, is the same, since the EPR parameters do not change. This can be observed by the overlay of the EPR lines in the high-field region, which is shown in Fig. 1b.

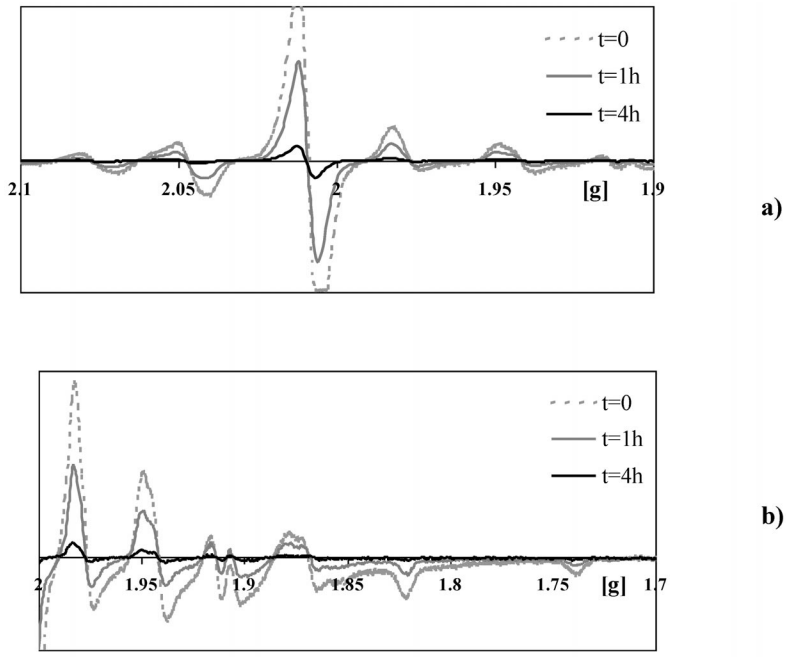


**Fig. 1** Change in the "frozen" EPR spectra of complex **7** with time: (a) central lines and (b) high field zone.

### $^{51}$V NMR

Complexes **7** and **8** were dissolved in DMSO (ca. 10 mM), and the solutions were left under air for ca. 4 h. The $^{51}$V NMR spectra of the complexes showed broad signals (W½ ~ 35 ppm) at –525 and –528 ppm for **7** and **8**, respectively (see Experimental section). The broadness of the resonances in DMSO is probably due to the high viscosity of the solvent and/or formation of several isomers. It should be emphasized that for the same solutions EPR spectra of reasonable intensity could be recorded.

The $V^V$ complexes **9** and **10** also display peaks with chemical shift values in the same region, although not exactly the same values, confirming that upon dissolving **9** and **10**, similar $V^V$ species form as those formed in solution after oxidation of the $V^{IV}O$ complexes **7** and **8**.

### Crystal structure of {[$V^VO${pyr(*S*,*S*-chen)}]$_2$(μ-O)$_2$}·2(CH$_3$)$_2$NCHO 11

Crystals of {$V^VO$[pyr(*S*,*S*-chen)]}$_2$(μ-O)$_2$ were obtained from a dimethylformamide (DMF) solution which contained complex **7** and were characterized by single-crystal X-ray diffraction. This is the result of the slow oxidation, partial hydrolysis of the ligand, and dimerization of the complex, which was probably driven by the electron deficiency and oxophilicity of the $V^V$ formed.

The asymmetric unit consists of one dinuclear molecule and two DMF [(CH$_3$)$_2$NCHO] molecules of crystallization. Figure 2 shows an ORTEP diagram of the dinuclear species with the atom-labeling scheme, and Table 2 contains selected bond lengths and angles. The two $V^V$ atoms are linked through two μ-oxo bridges, and the vanadium adopts a very distorted octahedral geometry with the ligand tricoordinated through the $O_{phenolate}$ and the two $N_{amine}$ atoms; the oxo and two bridging μ-oxo atoms complete the coordination sphere. The two cyclohexane rings display a chair conformation.

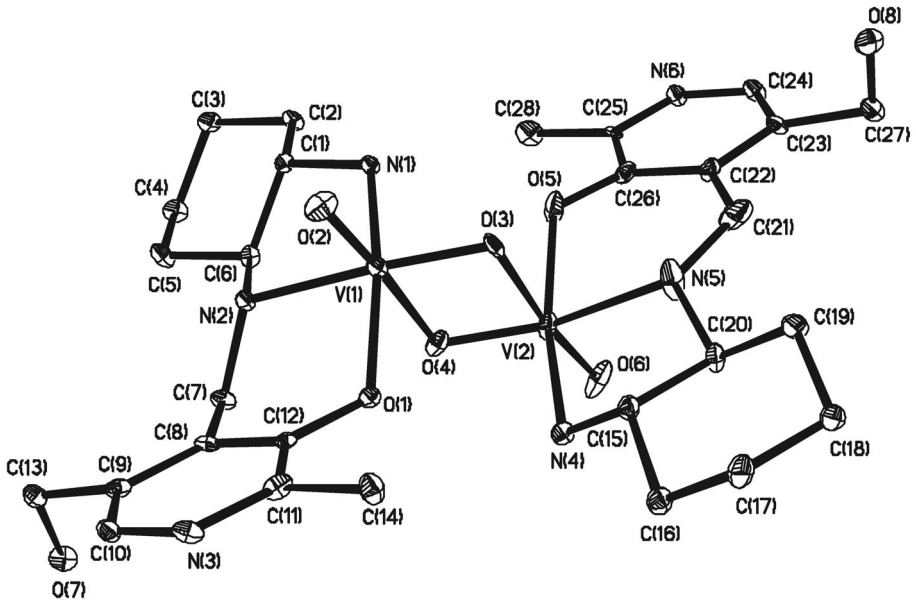


**Fig. 2** ORTEP diagram of $[\{V^{V}O[pyr(S,S\text{-chen})]\}_2(\mu\text{-}O)_2]\cdot 2(CH_3)_2NCHO$. The thermal ellipsoids are drawn at the 30 % probability level. The $(CH_3)_2NCHO$ molecules were omitted for clarity. The $N_{amine}$ atoms shown have *S*,*S* configuration.

**Table 2** Selected bond distances (Å) and angles (º) for **11**.

| $[\{V^{V}O[pyr(1S,2S\text{-chen})]\}_2(\mu\text{-}O)_2]\cdot 2(CH_3)_2NCHO$ | | | |
|---|---|---|---|
| Bond lengths (Å) | | Bond angles (º) | |
| N(1)–C(1) | 1.476(7) | C(7)–N(2)–C(6) | 114.1(4) |
| N(2)–C(6) | 1.499(7) | N(2)–C(7)–C(8) | 110.0(4) |
| N(2)–C(7) | 1.471(7) | C(21)–N(5)–C(20) | 115.5(5) |
| N(4)–C(15) | 1.487(7) | N(5)–C(21)–C(22) | 117.9(7) |
| N(5)–C(20) | 1.493(8) | O(2)–V(1)–O(3) | 105.7(2) |
| N(5)–C(21) | 1.395(9) | O(2)–V(1)–O(1) | 101.2(2) |
| O(1)–C(12) | 1.343(7) | O(3)–V(1)–O(1) | 100.0(2) |
| O(7)–C(13) | 1.428(6) | O(2)–V(1)–N(1) | 97.7(2) |
| V(1)–O(1) | 1.919(4) | O(3)–V(1)–N(1) | 91.0(2) |
| V(1)–O(2) | 1.615(4) | O(1)–V(1)–N(1) | 154.63(19) |
| V(1)–O(3) | 1.671(4) | O(2)–V(1)–N(2) | 93.1(2) |
| V(1)–O(4) | 2.337(4) | O(3)–V(1)–N(2) | 158.8(2) |
| V(1)–N(1) | 2.146(5) | O(1)–V(1)–N(2) | 85.58(18) |
| V(1)–N(2) | 2.245(5) | N(1)–V(1)–N(2) | 76.54(19) |
| V(2)–O(3) | 2.311(5) | O(2)–V(1)–O(4) | 173.4(2) |
| V(2)–O(4) | 1.665(5) | O(3)–V(1)–O(4) | 79.70(18) |
| V(2)–O(5) | 1.912(5) | O(1)–V(1)–O(4) | 81.41(16) |
| V(2)–O(6) | 1.607(5) | N(1)–V(1)–O(4) | 78.16(18) |
| V(2)–N(4) | 2.131(5) | N(2)–V(1)–O(4) | 80.95(17) |
| V(2)–N(5) | 2.213(7) | O(4)–V(2)–O(6) | 108.9(3) |

The two V=O bonds are very similar (average: 1.611 Å) and characteristic of oxo-type O atoms with strong π-bonding. The V–μ-oxo bonds *trans* to the secondary amine groups also show some

π-bonding character, presenting an average length of 1.668 Å. The V–μ-oxo bonds *trans* to the oxo groups are significantly longer (average: 2.324 Å). The V–V separation is 3.083 Å, comparable to the values found in related complexes [8]. The vanadium atom in each unit is displaced toward the apical oxo group from the equatorial plane defined by the $O_{phenolate}$, the two $N_{amine}$ groups, and the equatorial μ-oxo atom by 0.37 and 0.34 Å. The pyridinic rings are bent toward the terminal oxo groups, forming an angle of 35.6 and 26.23º with the plane defined by the donor atoms; and the alcoholate groups are in anti position to the oxo groups.

## CATALYTIC STUDIES

In order to screen the catalytic oxidative potential of the prepared complexes, they were applied in the oxidation of some simple organic molecules with $H_2O_2$. Three reactions were studied: the oxidation of styrene, cumene, and cyclohexene.

### Oxidation of styrene

The oxidation of styrene, catalyzed by the vanadium complexes, was carried out in acetonitrile using 30 % aqueous $H_2O_2$ as oxidant to give benzaldehyde (bza), 1-phenylethane-1,2-diol (phed), benzoic acid (bzac), and phenylacetaldehyde (phaa) (see Scheme 2). Reaction conditions were optimized considering **7** as a representative catalyst and varying the reaction parameters to achieve maximum oxidation of styrene.

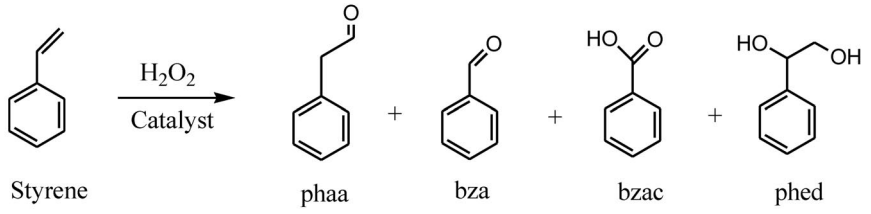


**Scheme 2** Products identified in the oxidation of styrene by $H_2O_2$ catalyzed by complexes **5–8**: phenylacetaldehyde (phaa), benzaldehyde (bza), benzoic acid (bzac), and 1-phenylethane-1,2-diol (phed).

Three different amounts viz. 0.1, 0.2, and 0.3 mmol of **7** were taken at the fixed amount of styrene (5 mmol), aqueous 30 % $H_2O_2$ (10 mmol) in $CH_3CN$ (10 ml), and the reaction was carried out at 80 °C. The obtained conversions (amount of styrene reacted) were plotted as a function of time and are presented in Fig. 3. The reaction conditions were also optimized varying the temperature (50–80 °C), and the amount of $H_2O_2$ (5, 10, and 15 mmol). The conversion increased with temperature, and at 80 °C the use of 10 mmol of aqueous 30 % $H_2O_2$, $CH_3CN$ (10 ml) and 0.1 mmol of catalyst were found optimum for the conversion of 5 mmol of substrate. Therefore, these reaction conditions were selected to carry out further catalytic studies.

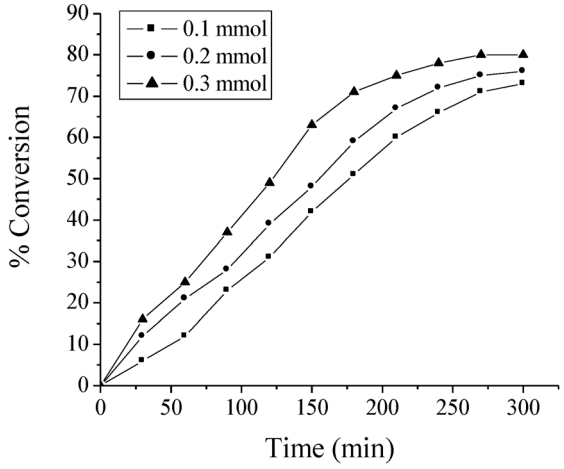


**Fig. 3** Effect of the amount of catalyst (mmol of **7**) on the oxidation of styrene. Reaction conditions: styrene (5 mmol), aqueous 30 % $H_2O_2$ (10 mmol), $CH_3CN$ (10 ml), and $T$ = 80 °C.

The conversions obtained by all catalysts, plotted as a function of time, are presented in Fig. 4. Table 3 provides details on the turnover frequency and selectivity of the various products obtained after 5 h of reaction time.

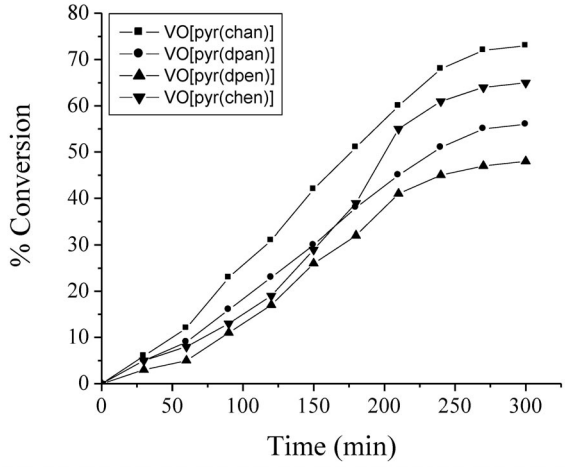


**Fig. 4** Oxidation of styrene catalyzed by various complexes as a function of time. Reaction conditions: catalyst (0.1 mmol), styrene (5 mmol), aqueous 30 % $H_2O_2$ (10 mmol), $CH_3CN$ (10 ml), and $T$ = 80 °C.

**Table 3** Percent conversion of styrene, turnover frequency (TOF), and product selectivity (see Scheme 2).

| | | | Selectivity[a], mol % | | | |
|---|---|---|---|---|---|---|
| Catalyst | Conversion (%) | TOF | phaa | bza | bzac | phed |
| VO[pyr(chen)] **5** | 65 | 6.5 | 5.2 | 85.3 | 7.4 | 2.1 |
| VO[pyr(dpen)] **6** | 48 | 4.8 | 2.3 | 91.7 | 0.7 | 5.3 |
| VO[pyr(chan)] **7** | 73 | 7.3 | 5.8 | 92.1 | 1.1 | 1.0 |
| VO[pyr(dpan)] **8** | 56 | 5.6 | 1.1 | 92.4 | 4.7 | 1.8 |

[a]phaa = phenylacetaldehyde, bza = benzaldehyde, bzac = benzoic acid, phed = 1-phenylethane-1,2-diol. Reaction conditions as mentioned in Fig. 4.

As shown in Table 3, complex **7** shows the highest catalytic activity with 73 % conversion of styrene, after 5 h, while **6** gave only 48 % conversion. Catalytic activities of other complexes vary within this range. Overall, V complexes with reduced ligands (V-pyran) perform better than with non-reduced ligands (V-pyren), and catalysts involving diaminocyclohexane-containing ligands are more active than those derived from diphenylethylenediamine. The most commercially interesting product, styrene oxide, is not found in the reaction products, probably because after its formation it was transformed into other products. The selectivity of benzaldehyde is the highest (>85 %), and this is possibly due to nucleophilic attack of $H_2O_2$ to styrene oxide, formed during the reaction, followed by cleavage of the hydroperoxystyrene intermediate. Benzaldehyde formation may also be facilitated by direct oxidative cleavage of the styrene side-chain double bond via a radical mechanism. The formation of benzoic acid through benzaldehyde is quite likely. Isomerization of styrene oxide may yield phenylacetaldehyde. Hydrolysis of styrene oxide to some extent by water present in $H_2O_2$ to 1-phenylethane-1,2-diol is also a plausible pathway for the formation of this product.

## Oxidation of cyclohexene

Under similar reaction conditions as those used for the oxidation of styrene, we have also carried out the oxidation of cyclohexene. Scheme 3 presents the isolated products; Fig. 5 shows the conversion plotted as a function of time, and Table 4 presents details on the product selectivity. Again, a very similar trend was obtained, i.e., highest conversion (71 %) with complex **7** and lowest (41 %) with **6**. Once again within the ligand system, the complexes with the pyran-type ligands have shown better performance than the complexes with the pyren-type ligands, but the most relevant difference is found in the type of diamine backbone, with the cyclohexanediamine derivatives showing conversions higher than 71 %, and the diphenyldiamine derivatives lower than 47 %. The selectivity of the reaction products follows the order: cyclohexane-1,2-diol > cyclohex-2-enol > cyclohex-2-enone ≈ 1,2-epoxycyclohexane. Thus, with a selectivity >70 %, cyclohexane-1,2-diol is the most important product and is probably the result of the oxidation of 1,2-epoxycyclohexane. A range of 11–18 % selectivity is found for the second highest product, cyclohex-2-enol. Epoxycyclohexane results from the oxidation of the double bond, while the allylic-oxidation pathway, forming cyclohex-2-enone and cyclohex-2-enol, reflects the preferential attack of the activated C–H bond over the C=C bond [30].

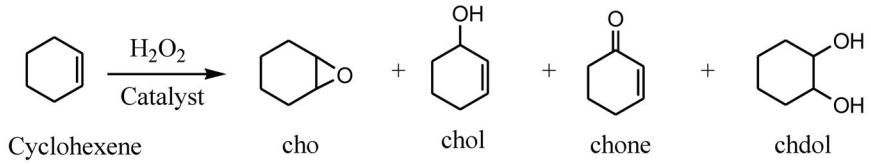


**Scheme 3** Products identified in the oxidation of cyclohexene by $H_2O_2$ catalyzed by complexes **5–8**: 1,2-epoxycyclohexane (cho), cyclohex-2-enol (chol), cyclohex-2-enone (chone), and cyclohexane-1,2-diol (chdol).

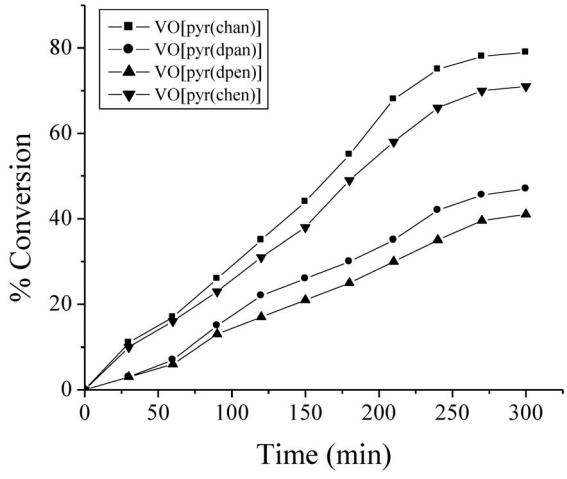


**Fig. 5** Oxidation of cyclohexene catalyzed by various complexes as a function of time. Reaction conditions: catalyst (0.1 mmol), cyclohexene (5 mmol), aqueous 30 % $H_2O_2$ (10 mmol), $CH_3CN$ (10 ml), and $T$ = 80 °C.

**Table 4** Percent conversion of cyclohexene, TOF, and product selectivity (see Scheme 3).

| | | | Selectivity[a], mol % | | | |
|---|---|---|---|---|---|---|
| Catalyst | Conversion (%) | TOF | cho | chdol | chol | chone |
| VO[pyr(chen)] **5** | 71 | 7.1 | 7 | 70 | 14 | 9 |
| VO[pyr(dpen)] **6** | 41 | 4.1 | 3 | 75 | 18 | 4 |
| VO[pyr(chan)] **7** | 79 | 7.9 | 5 | 79 | 5 | 1.0 |
| VO[pyr(dpan)] **8** | 47 | 4.7 | 4 | 78 | 13 | 5 |

[a]cho = 1,2-epoxycyclohexane, chdol = cyclohexane-1,2-diol, chol = cyclohex-2-enol, chone = cyclohex-2-enone. Reaction conditions as mentioned in Fig. 5.

## Oxidation of cumene

The oxidation of cumene gave acetophenone, 2-phenylpropanal, 1,2-epoxy-2-phenylpropane, and 2-phenylpropan-2-ol; Scheme 4. After several trials using 0.1 mmol of catalyst, the optimized reaction conditions for the maximum oxidation of 3 mmol of cumene were found to be aqueous 30 % $H_2O_2$ (9 mmol), acetonitrile (10 ml) at 80 °C, and the results reported were carried out under these conditions. Figure 6 presents the percentage of conversion as a function of time, and Table 5 provides other details.

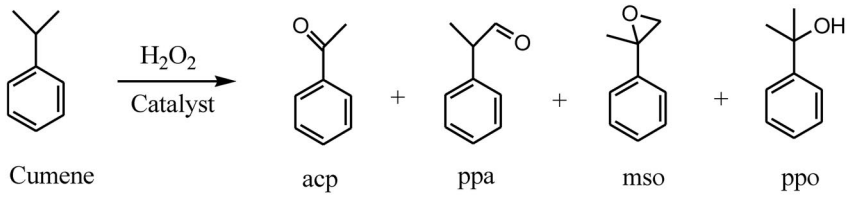


**Scheme 4** Products identified in the oxidation of cumene by $H_2O_2$ catalyzed by complexes **5–8**: acetophenone (acp), 2-phenylpropanal (ppa), 1,2-epoxy-2-phenylpropane (mso), and 2-phenylpropan-2-ol (ppo).

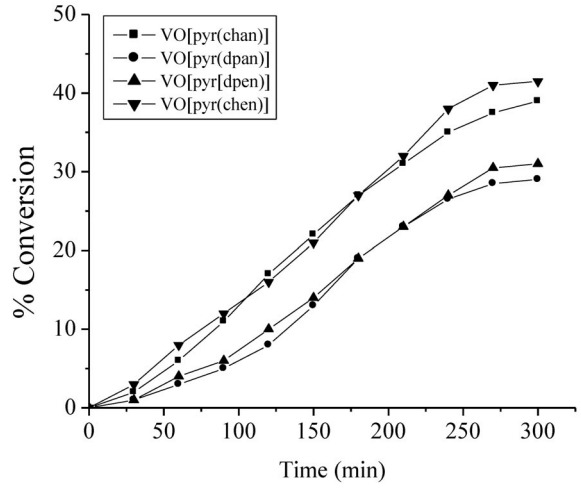


**Fig. 6** Oxidation of cumene catalyzed by various complexes as a function of time. Reaction conditions: catalyst (0.1 mmol), cumene (3 mmol), aqueous 30 % $H_2O_2$ (9 mmol), $CH_3CN$ (10 ml), and $T$ = 80 °C.

**Table 5** Percent conversion of cumene, TOF, and product selectivity (see Scheme 4).

| | | | Selectivity[a], mol % | | | |
|---|---|---|---|---|---|---|
| Catalyst | Conversion (%) | TOF | acp | ppa | mso | ppo |
| VO[pyr(chen)] **5** | 42 | 2.5 | 63 | 18 | 11 | 8 |
| VO[pyr(dpen)] **6** | 31 | 1.9 | 73 | 15 | 9 | 3 |
| VO[pyr(chan)] **7** | 39 | 2.3 | 65 | 21 | 8 | 6 |
| VO[pyr(dpan)] **8** | 29 | 1.7 | 55 | 20 | 6 | 19 |

[a]acp = acetophenone, ppa = 2-phenyl-2-propanal, mso = 1,2-epoxy-2-phenylpropane, ppo = 2-phenylpropan-2-ol. Reaction conditions as mentioned in Fig. 6.

In general, all complexes exhibited moderate catalytic activities between 29 to 42 % toward the oxidation of cumene. However, in contrast to other substrates studied here, the conversion of cumene by complexes of pyren ligands are 2–3 % better than the complexes of the reduced derivatives. Amongst the various products formed, the selectivity of an important product, acetophenone, is the highest and varies in the range 55–73 %, followed by 2-phenylpropanal with 15–21 %. The order of selectivity for two other products is: 1,2-epoxy-2-phenylpropane > 2-phenylpropan-2-ol, except for complex **8**.

## DFT studies

Several mechanisms have been proposed for the oxidation of alkenes (e.g., styrene) catalyzed by the vanadium complexes involving: (i) a transient vanadyl diradical species and the formation of a vanadium-peroxy-olefin intermediate; (ii) a simple bimolecular mechanism in which the nucleophile and the peroxo-metal complex react, i.e., a Sharpless-type mechanism; and (iii) the formation of a peroxo-metallocycle, i.e., a Mimoun-type mechanism which involves the coordination of an alkene molecule to the metal, followed by the formation of a penta-membered cyclic intermediate which decomposes onto the epoxide and catalyst.

To elucidate which of these epoxidation mechanisms is the most favorable, preliminary quantum-chemical calculations were done for the model complex [$V^{IV}O$(L)(ethylene)] as the starting material, where L = $^{-}$O–CH=CH–$CH_2$–NH–$CH_2$–$CH_2$–NH–$CH_2$–CH=CH–O$^{-}$ instead of the *N*,*N*′-ethylenebis-(pyridoxylaminato) ligand. In these studies, we are also considering the olefin as simply ethylene.

On the first step (see Scheme 5), the starting $V^{IV}$ complex **DFT-1** is oxidized by $H_2O_2$ to a $V^{V}$ complex **DFT-2**—the active species of the catalyst—which reacts further with another $H_2O_2$ molecule to form the peroxo-complex **DFT-3**. Both these reactions are well known in vanadium chemistry, and the corresponding mechanisms were considered previously by Shul'pin et al. [31] and by Khaliullin [32].

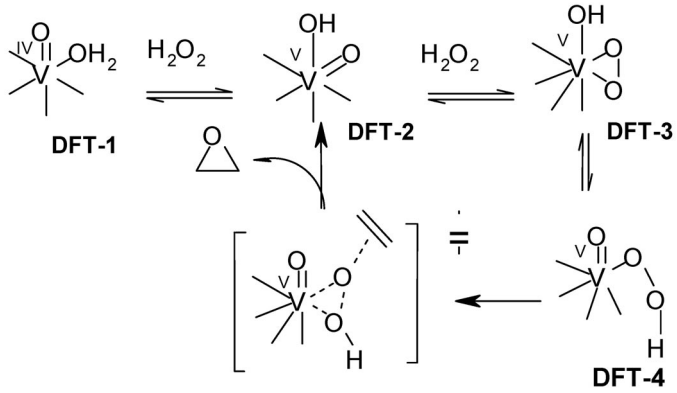


**Scheme 5** Outline of the most probable mechanism of alkene epoxidation catalyzed by the $V^{IV}$-salan complexes.

The calculations were carried out for the isomers in which two *O*-atoms and one *N*-atom of L occupy equatorial positions and another *N*-atom of L is in axial position. This isomeric form was found to be the most stable for the vanadium dioxo-*N*,*N*′-ethylenebis-(pyridoxylaminato) complexes on the basis of theoretical and experimental X-ray structural data [8]. The theoretical calculations done so far suggest that the Sharpless-type mechanism of alkene epoxidation involving the hydroperoxo species **DFT-4** is the most favorable one. More detailed theoretical mechanistic studies of olefin epoxidation catalyzed by vanadium complexes with reduced Schiff-base *N*,*O*-ligands will be reported [33].

## CONCLUSIONS

Two chiral salen-type and two chiral salan-type compounds were prepared and characterized. The corresponding $V^{IV}O$ complexes were prepared. Since they oxidize when dissolved in common organic solvents to $V^{V}$ species, the oxidation process was studied by spectroscopic techniques. The data support the assumption that a $VO_2^{+}$ center forms in solution, possibly transient $VO^{3+}$ being formed in the course of the oxidation process. Moreover, a crystal and molecular structure of a $V^{V}$ dinuclear species was ob-

tained, showing a $OV^{V}(\mu\text{-}O)_2V^{V}O$ core with two μ-oxo bridging atom, which gives further support to this assumption.

The complexes were applied as catalysts in the oxidation of simple substrates and showed good activities. Although most complexes did not show very good selectivity profiles, the V-salan complexes presented significantly better performance in the oxidation of styrene and cyclohexene than their V-salen counterparts.

As salan complexes are more stable than their salen counterparts, the salan systems may be promising for catalytic use, namely, after immobilization of the catalysts, and attempts to prepare immobilized catalysts with these systems are presently being carried out.

Preliminary DFT calculations were carried out with a model system to understand which is the more favorable mechanism in alkene epoxidation using salan systems as catalysts. The calculations suggest that a simple bimolecular mechanism where the nucleophile and the hydroperoxo-metal complex react, i.e., a Sharpless-type mechanism is the most favorable one, although the radical route, with a reaction pathway involving the generation of a diradical alkylperoxo intermediate, should also be competitive.

## SUPPLEMENTARY INFORMATION

Tables S1–S4 and Fig. S1 are available online (doi:10.1351/PAC-CON-08-09-07).

## ACKNOWLEDGMENTS

The authors wish to thank POCI 2010, FEDER and Fundação para a Ciência e Tecnologia (SFRH/BPD/13975/2003, PPCDT/QUI/55985/2004 and PPCDT/QUI/56949/2004) for financial support and the Spanish–Portuguese Bilateral Programme (Acção Integrada E-56/05, Acción Integrada HP2004-00).

## REFERENCES

1. T. Katsuki. *Coord. Chem. Rev.* **140**, 189 (1995).
2. L. Canali, D. C. Sherrington. *Chem. Soc. Rev.* **28**, 85 (1999).
3. (a) T. D. Cormac, M. R. Kenneth, M. W. Valerie, B. Claudine, G. G. Declan. *Top. Catal.* **V5**, 75 (1998); (b) P. G. Cozzi. *Chem. Soc. Rev.* **33**, 410 (2004); (c) J. F. Larrow, E. N. Jacobsen. *Top. Organomet. Chem.* **6**, 123 (2004).
4. (a) C. T. Cohen, T. Chu, G. W. Coates. *J. Am. Chem. Soc.* **27**, 10869 (2005); (b) H. Gröger. *Chem. Rev.* **103**, 2795 (2003); (c) G. M. Sammis, E. N. Jacobsen. *J. Am. Chem. Soc.* **125**, 4442 (2003); (d) W. Sun, H. Wang, C. Xia, J. Li, P. Zhao. *Angew. Chem., Int. Ed.* **42**, 1042 (2003); (e) G. M. Sammis, H. Danjo, E. N. Jacobsen. *J. Am. Chem. Soc.* **126**, 9928 (2004); (f) S.-X. Wang, M.-X. Wang, D.-X. Wang, Z. Zhu. *Angew. Chem., Int. Ed.* **47**, 388 (2008).
5. K. Nakajima, M. Kojima, J. Fujita. *Chem. Lett.* 1483 (1986).
6. M. Palucki, P. Hanson, E. N. Jacobsen. *Tetrahedron Lett.* **33**, 7111 (1992).
7. C. Kokubo, T. Katsuki. *Tetrahedron* **52**, 13895(1996).
8. I. Correia, J. Costa Pessoa, M. T. Duarte, R. T. Henriques, M. F. M. da Piedade, L. F. Veiros, T. Jakusch, T. Kiss, I. Dornyei, M. M. C. A. Castro, C. F. G. C. Geraldes, F. Avecilla. *Chem.—Eur. J.* **10**, 2301 (2004).
9. I. Correia, J. Costa Pessoa, M. T. Duarte, M. F. M. da Piedade, T. Jackush, T. Kiss, M. M. C. A. Castro, C. F. G. C. Geraldes, F. Avecilla. *Eur. J. Inorg. Chem.* 732 (2005).
10. A. Yeori, I. Goldberg, M. Shuster, M. Kol. *J. Am. Chem. Soc.* **128**, 13062 (2006).

11. Y. Sawada, K. Matsumoto, S. Kondo, H. Watanabe, T. Ozawa, K. Suzuki, B. Saito, T. Katsuki. *Angew. Chem., Int. Ed.* **45**, 3478 (2006).
12. H. Egami, T. Katsuli. *Angew. Chem., Int. Ed.* **129**, 8940 (2007).
13. H. Yang, H. Wang, C. Zhu. *J. Org. Chem.* **72**, 10029 (2007).
14. Y. Xiong, F. Wang, X. Huang, Y. Wen, X. Feng. *Chem.—Eur. J.* **13**, 829 (2007).
15. A. Yeori, S. Groysman, I. Goldberg, M. Kol. *Inorg. Chem*. **44**, 4466 (2005).
16. J. T. Sun, C. J. Zhu, Z. Y. Dai, M. H. Yang, Y. Pan, H. W. Hu. *J. Org. Chem.* **69**, 8500 (2004).
17. I. Correia, A. Dornyei, T. Jakusch, F. Avecilla, T. Kiss, J. Costa Pessoa. *Eur. J. Inorg. Chem.* 2819 (2006).
18. I. Correia, A. Dornyei, F. Avecilla, T. Kiss, J. Costa Pessoa. *Eur. J. Inorg. Chem.* 656 (2006).
19. P. Adão, J. Costa Pessoa, R. T. Henriques, M. L. Kuznetsov, F. Avecilla, M. R. Maurya, U. Kumar, I. Correia. *Inorg. Chem*. **48**, 3542 (2009).
20. N. Poddar, K. Day, S. C. N. Sarkar. *J. Indian Chem. Soc*. **40**, 489 (1963).
21. F. Galsbøl, P. Steenbøl, B. Søndergaard Sørensen. *Acta Chem. Scand.* **26**, 3605 (1972).
22. A. Rockenbauer, L. Korecz. *Appl. Magn. Reson.* **10**, 29 (1996).
23. N. D. Chasteen. In *Biological Magnetic Resonance*, J. Lawrence, L. J. Berliner, J. Reuben (Eds.), Chap. 2, p. 53, Plenum, New York (1981).
24. T. S. Smith, C. A. Root, J. W. Kampf, P. G. Rasmussen, V. L. Pecoraro. *J. Am. Chem. Soc.* **122**, 767 (2000).
25. A. J. Tasiopoulos, A. N. Troganis, A. E. Evangelou, C. P. Raptopoulou, A. Terzis, Y. Deligiannakis, T. A. Kabanos. *Chem.—Eur. J.* **5**, 910 (1999).
26. G. Micera, E. Garriba. *Dalton Trans.* 1914 (2009).
27. G. M. Sheldrick. *SHELXL-97: An Integrated System for Solving and Refining Crystal Strucutres from Diffraction Data (Revision 5.1)*, University of Göttingen, Germany (1997).
28. S. Bhattacharya, T. Ghosh. *Transition Met. Chem.* **27**, 89 (2002).
29. T. Ghosh, S. Bhattacharya, A. Das, G. Mukherjee, M. G. B. Drew. *Inorg. Chim. Acta* **358**, 989 (2005).
30. J. D. Koola, J. K. Kochi. *J. Org. Chem*. **52**, 4545 (1987).
31. G. B. Shul'pin, Y. N. Kozlov, G. V. Nizova, G. Süss-Fink, S. Stanislas, A. Kitaygorodskiy, V. S. Kulikova. *J. Chem. Soc., Perkin Trans. 2* 1351 (2001).
32. R. Z. Khaliullin, A. T. Bell, M. Head-Gordon. *J. Phys. Chem. B* **109**, 17984 (2005).
33. M. L. Kuznetsov, J. Costa Pessoa. *Dalton Trans.* In press, doi:10.1039/b902424g.